NeuroImage 59 (2012) 1988–1996

Contents lists available at SciVerse ScienceDirect

NeuroImage

journal homepage: www.elsevier.com/locate/ynimg

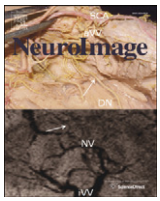

In vivo quantification of global connectivity in the human corpus callosum

Kevin Jarbo [a,c], Timothy Verstynen [a,b,*], Walter Schneider [a,b,c,d]

[a] *Learning Research and Development Center, PA, USA*
[b] *Center for the Neural Basis of Cognition, PA, USA*
[c] *University of Pittsburgh Medical Center, PA, USA*
[d] *Department of Psychology, University of Pittsburgh, Pittsburgh, PA, USA*

ARTICLE INFO

Article history:
Received 17 May 2011
Revised 3 September 2011
Accepted 21 September 2011
Available online 2 October 2011

Keywords:
Corpus callosum
Homotopic and heterotopic connectivity
Diffusion imaging

ABSTRACT

Histological studies on nonhuman primates have shown a rich topography of homotopic (i.e., going to the same regions) or heterotopic (i.e., going to different regions) callosal projections. Unfortunately, a complete within-subject mapping of commissural projections in humans has been limited due to the inability of typical imaging methods to detect lateral projections in posterior cortical regions. Here, we set out to map callosal projection connectivity, at the single subject level (N = 6), by combining high angular resolution diffusion weighted imaging and a novel multi-stage, region-of-interest (ROI) based fiber tracking approach. With these methods we were able to obtain a consistent increase in coverage of lateral projections to posterior cortical regions. Using 70 automatically segmented ROIs in each hemisphere and permutation statistics, we characterized significant interhemispheric connectivity patterns within each subject and observed: (1) consistent projections to frontal, parietal and occipital, but not temporal, areas, (2) a greater relative proportion of homotopic than heterotopic connections, and (3) commissural projections to the basal ganglia and thalamus that are consistent with human and nonhuman primate neuroanatomical literature. These results illustrate the first full connectivity analysis of the human corpus callosum, revealing several patterns consistent with histological findings in the nonhuman primate.

Introduction

The corpus callosum is the major interhemispheric commissure of the mammalian brain. In humans it consists of approximately 200 million axons connecting mostly homologous areas of the cortex in a nearly symmetrical fashion (Tomasch, 1954). Though, asymmetric heterotopic connections have also been identified (Locke et al., 1964; Fallon and Ziegler, 1979; Jones and Powell, 1969). Its broad cortical and subcortical connectivity and the wide range of physical and cognitive functions that is associated with (Bloom and Hynd, 2005), make the corpus callosum a critical white matter structure for clinicians and researchers alike. Studies on nonhuman primates have described three distinct regions of the corpus callosum: the genu, the body and the splenium (Schmahmann and Pandya, 2006). The genu and splenium are the most rostral and caudal sections of the corpus callosum, respectively, and continuous with the central body. More recently, it has been observed that humans exhibit a fairly similar midsagittal topography to the rhesus monkey (Hofer et al., 2008). While this three-segment view of callosal organization is widely accepted, alternative schemes for functional and anatomical organization of the corpus callosum consisting of five subdivisions have been presented (de Lacoste et al., 1985; Hofer and Frahm, 2006; Witelson, 1989), all of which have the body divided into anterior, central and posterior sections. The distribution of commissural fibers corresponds with the location of the contralateral cortical regions that they connect, e.g., fibers connecting the superior frontal gyrus primarily pass through the genu (Hofer and Frahm, 2006). Although distinct topographies of callosal projections based on current schemes have been presented (Chao et al., 2009; Park et al., 2008), *in vivo* visualization of commissural cortical tractography is far from complete due to limitations of current white matter imaging approaches.

Diffusion tensor imaging (DTI) has been shown to be useful in visualizing the white matter structure of the brain. Tractography based on DTI data has, so far, been sufficient in identifying major white matter pathways such as the corticobulbar and corticospinal tracts and association bundles including the superior longitudinal fasciculus and inferior occipitofrontal fasciculus (Hagmann et al., 2003). However, DTI has a limited capacity to resolve multiple crossings where fiber pathways intersect. This causes fiber tracking algorithms to miss certain well known pathways during the tracking process, when pathways project through voxels with complex crossing patterns (Weeden et al., 2008). Unfortunately, this is particularly problematic for the corpus callosum, since its axons intersect and interdigitate with fibers from up to four other major pathways, e.g.,

* Corresponding author at: University of Pittsburgh Learning Research and Development Center, 3939 O'Hara St Ste., 630, Pittsburgh, PA 15620, USA. Tel.: +1 412 624 1194.
E-mail address: timothyv@pitt.edu (T. Verstynen).

1053-8119/$ – see front matter © 2011 Elsevier Inc. All rights reserved.
doi:10.1016/j.neuroimage.2011.09.056

superior longitudinal fasciculus, corticospinal tract, corona radiata, as well as intralobular association fibers (Dougherty et al., 2005). Thus the resolution of callosal fibers with typical fiber tracking approaches has, thus far, been limited when compared with a comprehensive literature on human and nonhuman primate histological and imaging data (Schmahmann and Pandya, 2006).

Recently, the use of high angular resolution diffusion imaging (HARDI) and multi-shell techniques (Tuch, 2004) such as diffusion spectrum imaging (DSI; Weeden et al., 2008) have been implemented with some degree of success at dealing with the fiber crossing problem (Chao et al., 2009; Descoteaux et al., 2009). However, beyond better angular resolution, one primary limitation in characterizing callosal pathways rests in the nature of the tractography approach used by most researchers. A whole brain tracking approach, where all voxels in the brain are used as seeds in the tracking process and relevant fibers selected *post hoc*, exacerbates the crossing problem because the major fiber direction within a voxel dominates the tracking process. This introduces biases in the detection of fiber pathways and limits coverage. For example, the lateral callosal projections connecting ventral portions of the superior parietal lobule and the whole of the inferior parietal lobule are consistently missed, even though these pathways are known to exist (Selemon and Goldman-Rakic, 1988). Even as the resolution of these techniques have improved, no current whole-brain approaches to cortical tractography can resolve this coverage issue with callosal projections to posterior regions of the brain.

Here, we use a collection of imaging and reconstruction approaches designed to optimize the spatial resolution of tractography data, to a sub-voxel resolution, and resolve complex fiber crossings. This optimized pipeline includes a high-directional DSI acquisition, with generalized q-sampling imaging (GQI) reconstruction and a streamline tracking technique that uses a neighborhood interpolation process on the orientation diffusion functions of underlying water diffusion (Yeh et al., 2010). Through this unique combination of approaches, we can reliably track fibers to and from cortical and subcortical regions, through complex fiber crossings with a sub-voxel resolution approaching the sub-millimeter level. We refer this type of approach as High Definition Fiber Tracking (HDFT; Verstynen et al., 2011) in order to differentiate it from the relatively lower directional DTI methods that are typically used for voxel-wise analytical approaches and tractography of larger, single-fiber pathways. To compensate for the considerably low detectability of posterior commissural projections, we coupled HDFT with a multi-stage, region of interest (ROI) based tractography approach designed to optimize detection of commissural tracts to specific areas of cortex. Applying a permutation statistical analysis, we were able to identify significant connectivity patterns on the single subject level. These connectivity maps revealed both heterotopic and homotopic projection patterns that were consistent with invasive histological mapping studies.

Methods and materials

Participants

Six neurologically healthy adults (2 female; all right-handed; ages 22–31) from the University of Pittsburgh community participated in this study. Two of the participants were tested as part of a larger data collection effort associated with the 2009 Pittsburgh Brain Competition. All participants were prescreened prior to scanning to rule out any contraindications to MR imaging. Written consent was obtained from all participants prior to scanning in accord with approval by the University of Pittsburgh's Institutional Review Board. Participants were financially compensated for their participation. Diffusion imaging data on other fiber pathways have previously been reported in five of the six subjects reported here (Verstynen et al., 2011).

Image acquisition and reconstruction

Diffusion spectrum imaging (DSI) data were acquired on 3,T Tim Trio Systems (Siemens, Inc.) using a 32-channel coil. A 257-direction scan using a twice-refocused spin-echo EPI sequence and multiple q-values (TR = 9916 ms, TE = 157 ms, voxel size = 2.4 × 2.4 × 2.4 mm, FoV = 231 × 231 mm, b-max = 7000 s/mm^2, 5 shells). Because DSI is a multi-shell sequence, multiple b-values were used, ranging from 300 to 7000 s/mm^2. A generalized q-sampling imaging (GQI) approach using a half-sphere scheme (Yeh et al., 2010) was used to reconstruct DSI data using DSI Studio (http://dsi-studio.labsolver.org). No motion or eddy current distortion correction was applied to the images. The orientation distribution functions (ODFs) were computed with a mean diffusion distance of 1.2 and allowing for 4 reconstructed fiber directions per voxel.

For high resolution anatomical comparisons, we also included a 9-minute T1-weighted axial MPRAGE sequence (TR = 2110 ms, TE = 2.63 ms, flip angle = 8°, 176 slices, FoV = 256 × 256 mm, voxel size = 1.0 × 1.0 × 1.0 mm).

Anatomical segmentation and ROI registration

FreeSurfer (http://surfer.nmr.mgh.harvard.edu) was used to automatically segment cortical, subcortical and callosal ROIs based on previous brain atlases (Fischl et al., 2002) using each participant's T1-weighted MPRAGE image. Table 1 lists the ROIs grouped by lobe, as well as subcortical ROIs selected for each hemisphere. The corpus callosum for each dataset was automatically segmented into five divisions: anterior, mid-anterior, central, mid-posterior, and posterior (Fischl et al., 2002). Each ROI was segmented from the atlas template and saved as individual NIfTI files. Custom MATLAB scripts were used to extract the b0 image for each dataset from the raw DSI data. A linear, rigid body transformation procedure in SPM8 was then used to coregister the ROIs to each participant's b0 image and resliced to have the same voxel and matrix dimensions as the DSI data. The

Table 1
Seventy FreeSurfer regions-of-interest (ROIs) per hemisphere.

Frontal: 28 regions	Frontomarginal gyrus and sulcus, transverse frontopolar gyrus and sulcus, inferior frontal gyrus (opercular), inferior frontal gyrus (orbital), inferior frontal gyrus (triangular), middle frontal gyrus superior frontal gyrus, orbital gyrus, precental gyrus, rectus gyrus, horizontal lateral fissure, vertical lateral fissure, central sulcus, inferior frontal sulcus, middle frontal sulcus, superior frontal sulcus, lateral orbital sulcus, medial olfactory orbital sulcus, H-shaped orbital sulcus, inferior precentral sulcus, superior precentral sulcus, suborbital sulcus, anterior cingulate gyrus and sulcus, middle anterior cingulate gyrus and sulcus, middle posterior cingulate gyrus and sulcus, insula and superior central insula, short insular gyrus, cingulate marginalis sulcus
Parietal: 13 regions	Inferior parietal lobule (angular gyrus), inferior parietal lobule (supramarginal gyrus), superior parietal lobule, postcentral gyrus, precuneus, posterior lateral fissure, Jesden's sulcus, intraparietal sulcus, parieto-occipital sulcus, postcentral sulcus, subparietal sulcus, dorsal posterior cingulate gyrus, ventral posterior cingulate gyrus
Occipital: 11 regions	Inferior occipital gyrus and sulcus, cuneus, lingual gyrus, middle occipital gyrus, superior occipital gyrus, occipital pole, calcarine sulcus, posterior collateral sulcus, middle occipital and lunate sulci, superior and transverse occipital sulci, anterior occipital sulcus
Temporal: 13 regions	Lateral fusiform gyrus, medial parahippocampal gyrus, inferior temporal gyrus, middle temporal gyrus, transverse superior temporal gyrus, lateral superior temporal gyrus, temporal pole, transverse anterior collateral sulcus, lateral occipito-temporal sulcus medial and lingual occipito-temporal sulcus, inferior temporal sulcus, superior temporal sulcus, transverse temporal sulcus
Subcortical: 5 regions	Amygdala, caudate, pallidum, putamen, thalamus

resliced ROIs were used as masks during the tractography and fiber track analysis processes described in the following sections.

Fiber tractography

All fiber tracking on DSI datasets was done with DSI Studio using an ODF-streamlined, multi-FACT deterministic tractography method (Yeh et al., 2010). As an initial assessment of baseline coverage, we first performed whole brain tractography on each dataset. Using a random seeding approach, we initiated tracking from arbitrary locations within all brain voxels, with the initial direction randomly selected. Fiber progression continued with a step size of 1.0 mm. To smooth each track, the next directional estimate of each voxel was weighted as a percentage of the incoming direction of the fiber (see Table 2). The tracking was terminated when the relative FA for the incoming direction dropped below a preset threshold (Table 2) or exceeded a turning angle of 75°. The FA termination threshold was adjusted on a per subject basis depending on the relative signal to noise of each scan. Rather than extract a subset of callosal fibers from a larger set of whole brain fibers, we continued the sampling process until a specific number of callosal fibers were identified (Table 2), based on a midsagittal ROI of the corpus callosum. All other fibers were discarded. These maps were used to visually compare the coverage obtained using a ROI-based approach and are shown in Supplementary Fig. 1.

To optimize coverage for our connectivity analysis, we adopted a two-stage, hybrid tractography approach. In the first stage, we manually drew a ROI mask over a single slice of the corpus callosum on the plane of the longitudinal fissure for each dataset and tracked 132,000 fibers meeting specific criteria (see Table 2) through the callosal ROI from a whole brain seed mask automatically generated by DSI Studio. These tracks were saved and visualized in TrackVis (Wang et al., 2007), which was then used to isolate fibers projecting through each of the five divisions of the corpus callosum (see Supplementary Fig. 1). The endpoint distributions of these streamlines were saved in volume space by calculating the density of fibers that terminated within each voxel of the brain. These distribution maps were then used to determine where to create ROI masks of regions of low-detectability commissural projections (LDCPs; Fig. 1b). LDCP masks were manually drawn for each dataset on axial slices of a generalized fractional anisotropy map generated by DSI Studio.

Each mask encompassed the entire lateral surface of parietal cortex and was expanded by one voxel in all directions to maximize coverage of the region and compensate for partial-voluming effects. Thus, masks contained anterior aspects of the lateral occipital gyri and the most posterior portions of the superior and middle temporal gyri. After this, a second set of tracking was performed using the LDCP output masks generated from the first stage of tractography. The LDCP regions typically included the lateral parietal cortex, most prominently the inferior parietal lobule (IPL), anterior portions of the occipital lobe and posterior temporal cortex. We expected projections to be detected in all of these areas based on comparative literature on primate neuroanatomy and post-mortem dissection and staining research (Hofer et al., 2008). As before, we adopted a whole-brain seeding method, but only accepted fibers that passed through the corpus callosum from one LDCP mask.

Tractography was performed independently for the left and right hemisphere LDCP masks. In all subjects we tried to obtain up to 32,000 fibers projecting to each LDCP mask; however, in some subjects we could only obtain up to 18,640 fibers (range = 18,640 to 31,380) before encountering system memory limitations in the analysis computer used. In order to maximize detectability, the turning angle threshold was reduced to 45° to ensure that the lateral fibers would be tracked while ignoring dorsal projections to areas like the superior parietal lobule (SPL) and ventral projections to the superior temporal gyrus (STG). Refer to Table 2 for a listing of dataset-specific parameters for each track reconstruction. Theoretically, the low diffusion signal in the direction of fibers continuing to the LDCP regions (see Fig. 1a and Results 3.1.1) means that increasing the sampling of fibers should increase the number of observed streamlines that meet criteria. By ignoring all but these fibers we obtain a selective set of streamlines in areas with low signal-to-noise. These new tractography files were combined with the fibers from the first stage of tracking using the track_merge function of TrackVis (Wang et al., 2007) to show where multiple fiber crossings and decussations occurred.

Table 2
Optimized parameters* for Stage 1 and individual low-detectability commissural projection (LDCP) tractography.

Subj.	Actual # of fibers tracked	Region	FA threshold	Smoothing
1	132,000	Whole brain	0.0600	0.60
1	20,000	Left LDCP	0.0625	0.40
1	20,000	Right LDCP	0.0625	0.40
2	132,000	Whole brain	0.0582	0.60
2	29,011	Left LDCP	0.0775	0.75
2	5177	Right LDCP	0.0775	0.75
3	132,000	Whole brain	0.0631	0.65
3	20,000	Left LDCP	0.0465	0.60
3	20,000	Right LDCP	0.0465	0.60
4	132,000	Whole brain	0.0369	0.70
4	19,625	Left LDCP	0.0575	0.80
4	18,640	Right LDCP	0.0500	0.80
5	132,000	Whole brain	0.0457	0.70
5	31,380	Left LDCP	0.0275	0.75
5	29,221	Right LDCP	0.0275	0.75
6	132,000	Whole brain	0.0715	0.70
6	28,601	Left LDCP	0.1460	0.50
6	31,065	Right LDCP	0.4186	0.40

*The following parameters and corresponding values or settings were the same for all datasets: reconstruction method, GQI; ODF dimensions, 642 directions (8-fold); number of fibers per voxel, 4; sampling length, 1.2 mm; turning angle 75° (whole brain) and 45° (LDCPs); trilinear interpolation; step size, 1 mm; fiber length constraint, 30–150 mm.

Data analysis

In order to quantify the connectivity pattern of each participant's callosal projections, we used an iterative mapping approach. For mapped fibers from both the first and second stages of the tracking process we categorized start and end locations of each fiber as being in any of the 140 target ROIs (70 per hemisphere). Fibers were only categorized if their start or endpoints were *within* the target ROI mask. This process resulted in an *NxF* binary matrix, $\boldsymbol{M}$, where N is the number of target ROIs (i.e., 140, ordered by hemisphere and then lobe) and F is the number of tracked fibers in the dataset. Because the ROI masks were both expanded by one voxel and downsampled from 1 mm^3 to 2.4 mm^3 space, there was some overlap of neighboring masks and thus some fibers could have more than one endpoint classification (13% of fibers on average). Indeed, only a subset of these overlap fibers projected to similar regions in the contralateral hemisphere, thus having a minimal influence on subsequent connectivity estimates. Since region classifications are based on folding geometry, not underlying cytoarchitectonics, the spatial nature of this overlap pattern will also vary across subjects. This means that including this variance only makes subsequent group connectivity maps more conservative, not less. Therefore, these dual connections were kept for subsequent analysis. To determine the connectivity map of callosal projections, $\boldsymbol{C}$, we isolated the upper-right quadrant of the dot-product of the connectivity matrix (i.e., $\boldsymbol{C} = ½ * \boldsymbol{M}\boldsymbol{M}^{T}$). In this way $\boldsymbol{C}$ identifies the number of fibers that project from an ROI in the left hemisphere (rows) and terminate in a region in the contralateral hemisphere (columns).

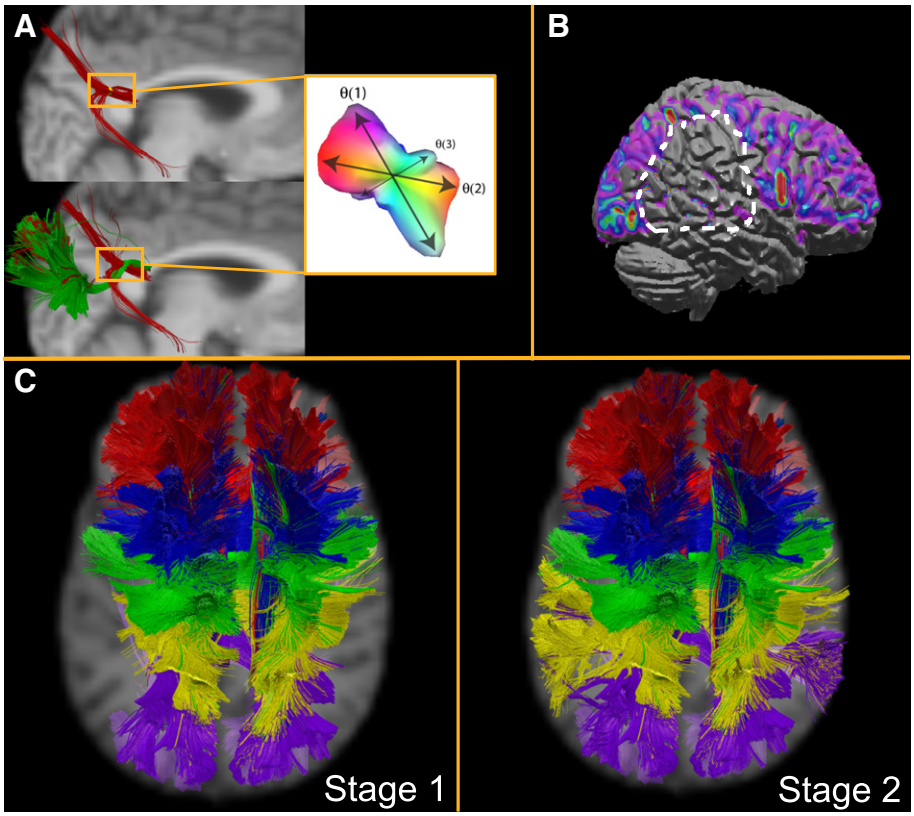

Fig. 1. Tractography coverage results. A) Bifurcating fibers were observed in a region with a complex fiber crossing (upper left inset). Only two fiber pathways are detected from a whole brain seeding approach (i.e., Stage 1) because of the two stronger diffusion directions in the ODF (θ(1) and θ(2) in right inset). Fibers in the less dominant third pathway (θ (3)) are only detectable after using a restricted ROI based tractography (i.e., Stage 2; green fibers). B) Smoothed heat map of fiber endpoints at the cortical surface (normalized into MNI-space for display purposes). The loss of coverage to posterior regions, i.e., the LDCP areas, is outlined. C) Initial coverage from a whole brain seeded tractography (left) and the combined whole brain with restricted ROI fibers for an example subject. Fibers are colored based on whether they pass through the genu (red), anterior trunk (blue), medial trunk (green), posterior trunk (yellow) or splenium (violet) sections of the corpus callosum.

In order to identify the probability of getting a particular ***C*** by chance, we adopted a permutation test approach (Manly, 1997). To do this, we simulated a random ***C*** by permuting the column entries of ***M***. This was done 100 times for each dataset to estimate the mean and standard deviation of the chance distribution at each connection pair (i.e., each *i*, *j* entry of ***C***). The observed values of ***C*** were then converted into z-score units using these mean and standard deviation matrices reflecting the null distribution. Any entry in ***C*** with a value greater than 1.96 was then determined to be a significant connection (i.e., $p<0.05$). The final ***C*** matrices for every individual subject are shown in Supplementary Fig. 2.

Results

Improved coverage of commissural projections

We first compared the change in callosal tractography results obtained with and without using the LDCP masks. Across all participants, Stage 1 reconstruction resulted in a substantial lack of coverage of fiber projections to the inferior parietal lobule (IPL) and nonspecific regions of the anterior occipital lobe (Fig. 1a). This is inconsistent with histological literature showing these projections exist (de Lacoste et al., 1985). We observed few projections from the posterior temporal lobe and none of these were more ventral or anterior than the caudal aspects of the superior temporal gyrus (STG). However, this is to be expected since the majority of interhemispheric temporal projections pass through the anterior commissure (Di Virgilio et al., 1999).

The lack of coverage to these posterior parietal and occipital regions indicates that fibers passing through the posterior body and splenium suffer from a crossing problem, impairing cortical coverage. To get a better understanding of the etiology of this problem, we looked at projections passing through the posterior body and splenium and identified a consistent triple-crossing region, i.e., at least three fiber pathways passing through the same voxel. Fig. 1a shows the ODF of an example voxel in this region for one subject. This example ODF shows two dominant fiber projections (i.e. θ(1) and θ(2)) and a third weaker anisotropy oriented towards the lateral parietal regions (i.e., θ(3)). A close examination of fibers passing through this region (Fig. 1b) revealed that most fibers follow the diffusion directions toward the superior temporal gyrus (STG), or of the tapetum, and the superior temporal lobule (SPL). Almost no fibers projecting toward the ventral parietal regions were detected past this triple crossing area.

Adding the LDCP restricted tractography (i.e., Stage 2, see Methods subsection Fiber tractography) resulted in a significant increase in detection of fibers to lateral posterior regions (Fig. 1a green fibers). Upon visual inspection, we saw improved fiber detection in parietal, occipital and temporal projections running through the splenium and posterior mid-section of the corpus callosum (purple and yellow fibers in Fig. 1c). This was consistently seen in all 6 subjects (Supplementary Fig. 1). To quantify this improved coverage we looked at the change in interhemispheric connectivity matrices, ***C***, before and after adding the LDCP restricted tractography results. Fig. 2a shows the average z-score change across all ROI pairs. The most notable increase in observed connections is in the parietal lobes, which is where the primary regions of low detectability were observed. To better quantify

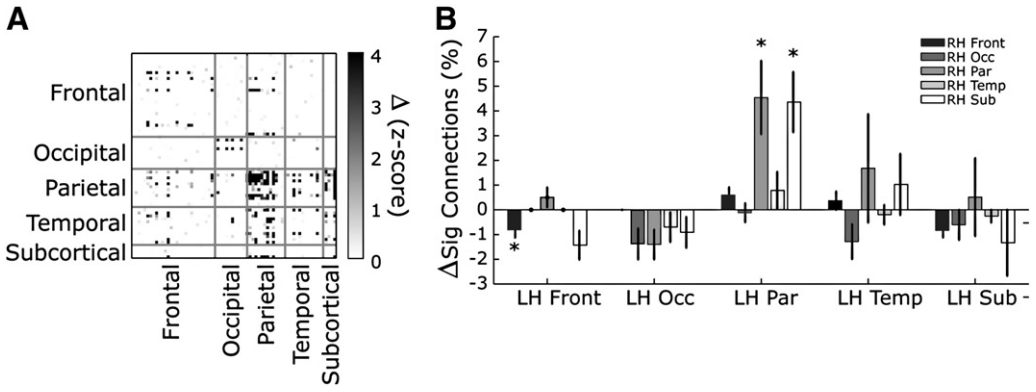

Fig. 2. Quantification of improved coverage with LDCPs. A) Average change in the connectivity matrix, ***C***, after applying the ROI restricted tractography. Rows show left hemisphere ROIs and columns show right hemisphere regions. B) Change in the number of significant projections for every lobular pair (i.e., significant connections for every sub-matrix shown in *A*). Error bars reflect standard error across subjects and asterisks reflect $p<0.05$. See text for statistical values.

this, we looked at the average change in significant projections between and across lobes (i.e., for each sub-matrix in Fig. 2a) after adding in the LDCP restricted fibers (Fig. 2b). As expected, there was a consistent improvement in the parietal connections ($T(5)=3.05$, $p<0.025$) and parietal-to-subcortical connections ($T(5)=3.58$, $p<0.025$). Fortunately, adding the LDCP restricted tractography did not significantly influence the overall connectivity structure in any other region pairs, with the exception of frontal-to-frontal connections that showed a very slight decrease in the number of significant connections ($T(5)=-2.56$, $p<0.05$).

Callosal connectivity mapping

After observing an increase in commissural projection coverage in posterior regions of the brain, we next examined those projections for consistency with the literature regarding homotopic and heterotopic connectivity. Fig. 3a shows the average connectivity pattern observed across all subjects and all cortical and subcortical ROI masks. A high degree of significant homotopic interlobular connections, represented by regions along the diagonal of Fig. 3a, were observed for the frontal, parietal and occipital lobes. Fig. 3b shows the average number of connected region pairs for each sub-matrix of Fig. 3a. Overall, the homotopic projections between the major lobes were significant for the frontal, occipital and parietal areas. In each of these lobes we also observed significant projections to subcortical targets (detailed in Results subsection Subcortical connectivity). In contrast, virtually no homotopic or heterotopic projections were detected in the temporal lobes. This is, however, expected since these interhemispheric projections emanate through the anterior commissure (Di Virgilio et al., 1999). For this reason, we excluded temporal lobe regions from further interhemispheric connectivity analysis.

Frontal connectivity

We examined the connectivity of 28 ROIs in the frontal lobe, shown in Fig. 4a with the left hemisphere regions labeled along the vertical axis (i.e., rows) and those in the right on the horizontal axis (i.e., columns). Each entry in this matrix shows the percentage of participants that had statistically significant connections between each interhemispheric ROI pair. The middle frontal gyrus showed the highest amount of overall contralateral connectivity, with all subjects showing significant homotopic connectivity. In fact, the frontal lobe regions showed a high degree of overall connectivity, with only three ROIs showing no significant heterotopic connections to any contralateral area.

We next looked at the relative prevalence of homotopic and heterotopic projections within the frontal lobe. All homotopic ROIs are located along the diagonal axis of Fig. 4a, whereas heterotopic regions are all off-diagonal entries. The percentage of significant homotopic and heterotopic projections, across subjects, is shown in Fig. 4b. Overall, homotopic regions had a higher degree of consistent connections than heterotopic (paired $T(5)=7.25$, $p<0.001$), but this may not be

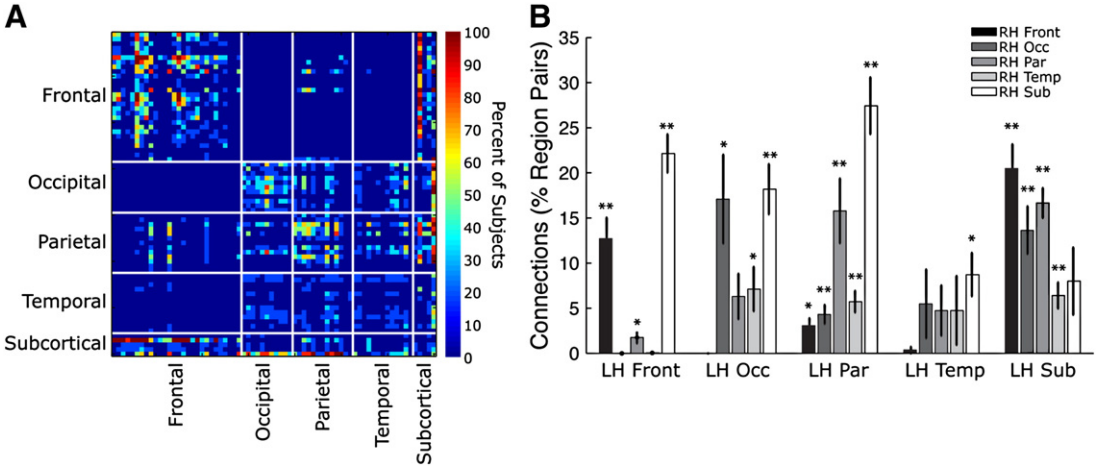

Fig. 3. Overall connectivity summary. A) Pairwise connections for all target ROIs shown as percent of subjects with significant connections for each pair (i.e., each entry in the matrix). Rows are left hemisphere ROIs and columns are right hemisphere. B) Average lobular homotopic and heterotopic projections (i.e., average number of significant pairs for each sub-matrix in *A* across subjects. Error bars show standard error across subjects. Single asterisks reflect $p<0.025$ and double asterisks reflect $p<0.005$ of the 1-sample *t*-test comparing the observed fibers to a null of 0 fibers.

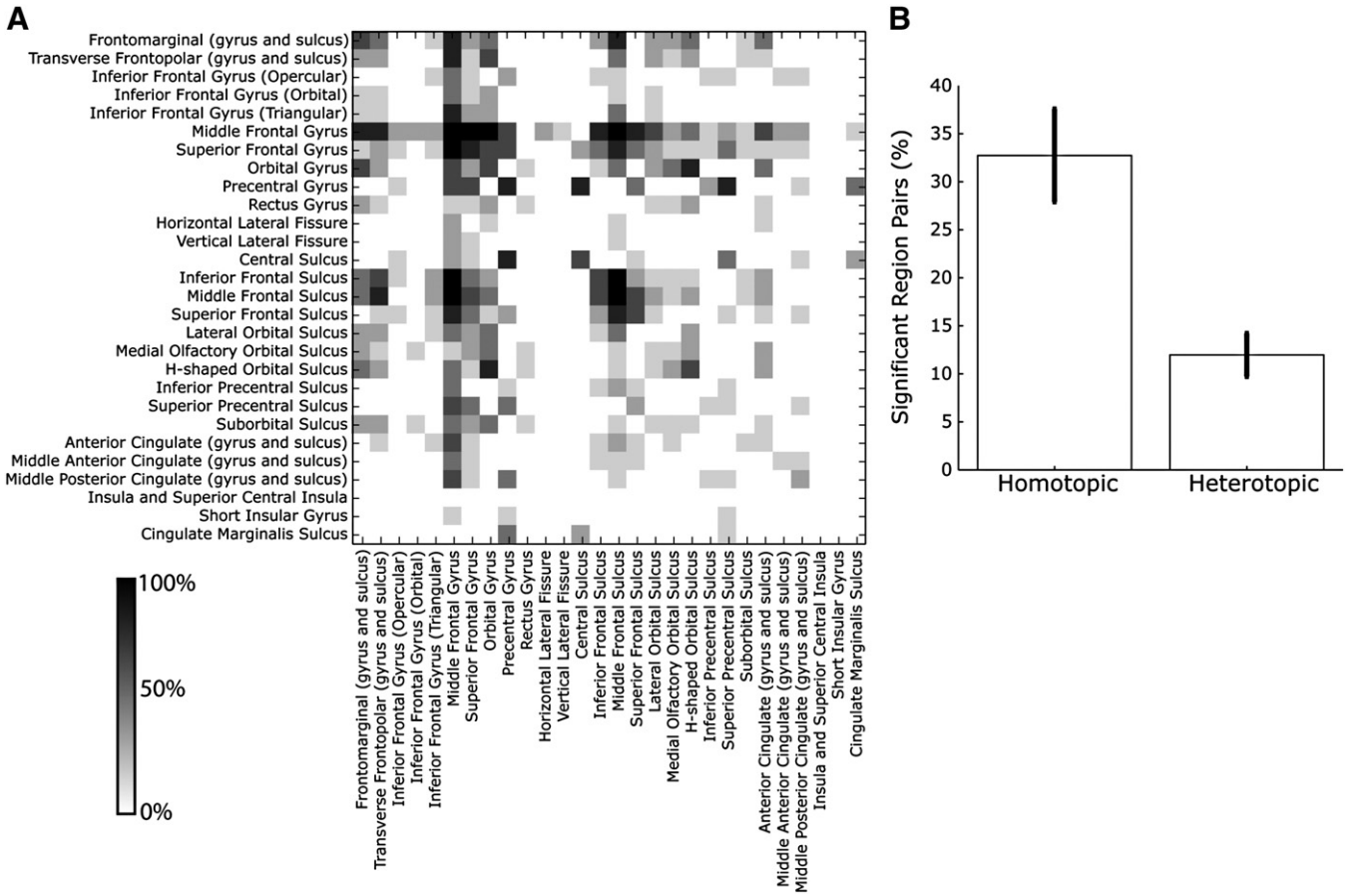

Fig. 4. Frontal lobe connectivity. A) The connectivity matrix ***C*** for all 28 frontal ROIs. Values reflect percent of subjects with statistically significant connections. B) Average number of significant homotopic (i.e., diagonal entries in A) and heterotopic projections (i.e., off diagonal entries) within frontal regions. Error bars reflect standard error across subjects.

surprising given that there were 28 times more heterotopic pairs than homotopic.

Occipital connectivity

We next looked at the connectivity between 11 pairs of occipital lobe ROIs (Fig. 5a). The greatest amount of consistent connectivity was found between the occipital poles of each hemisphere, which had the highest percentage of homotopic and heterotopic projections across all datasets. This observation is consistent with research on V1 in the visual system (Di Virgilio and Clarke, 1997) including imaging studies showing retinotopic organization of these fibers using DTI (Dougherty et al., 2005). Moreover, a high degree of consistent homotopic and heterotopic connectivity can be seen between the middle occipital gyrus, superior occipital gyrus, occipital pole and calcarine sulcus, which is also consistent with histological literature on the human visual system (Clarke and Miklossy, 1990). Similar to frontal areas, occipital regions had a higher consistency of homotopic than heterotopic projections (Fig. 5b; paired $T(5) = 3.20$, $p = 0.01$), but again this may be biased by the larger number of heterotopic pairs.

Parietal connectivity

13 pairs of ROIs were used in our analysis of parietal lobe connectivity. In general, parietal regions had a high degree of consistent connectivity (Fig. 6a). This was particularly strong in the precuneus, which showed regular connectivity across subjects to several contralateral ROIs, especially the superior and inferior parietal lobules and the postcentral gyrus and sulcus. The postcentral gyri and sulci showed nearly the exact same broad pattern of significant connectivity with other parietal lobes ROIs across all datasets. The only difference occurred between the left ventral posterior cingulate gyrus and right postcentral sulcus. Most prominently, no significant connections between the right dorsal or ventral posterior cingulate gyrus and left Jensen's sulcus to any contralateral parietal ROI were observed. Left and right supramarginal gyri ROIs showed only significant homotopic connections in fewer than half of subjects and no significant heterotopic connectivity in any dataset. Consistent with the other lobes, inter-parietal pathways had more consistent homotopic than heterotopic pairs (Fig. 6b; paired $T(5) = 3.66$, $p = 0.007$).

Subcortical connectivity

Previous work has shown that beyond just cortical–cortical connections, the corpus callosum also contains fibers that connect cortical to contralateral subcortical nuclei, specifically the thalamus and striatum (Cummings, 1993). We looked at these projections for all subjects and included two control regions, the amygdala and pallidum, as control areas that should not exhibit callosal connectivity. We observed significant commissural connectivity from all lobes to the striatum and thalamus that is consistent with current literature (for review see Chapters 8 and 14 Nieuwenhuys et al., 2007). Fig. 7 shows the average number of significant connections across subjects from cortical to contralateral subcortical ROIs. Overall, we see a high degree of connectivity between cortical regions and the caudate and thalamus. In both hemispheres, the caudate was consistently connected with frontal areas (Left: $T(5) = 7.01$, $p < 0.025$; Right: 5.82, $p < 0.025$) with over 65% of frontal ROIs projecting to the contralateral striatum which is consistent with primate literature on corticostriatal projections (Selemon and Goldman-Rakic, 1988). Interestingly, we found that the right caudate was also consistently connected to about 40% of the left hemisphere parietal ROIs ($T(5) = 2.71$, $p < 0.025$). These striatal projections only appeared to terminate on

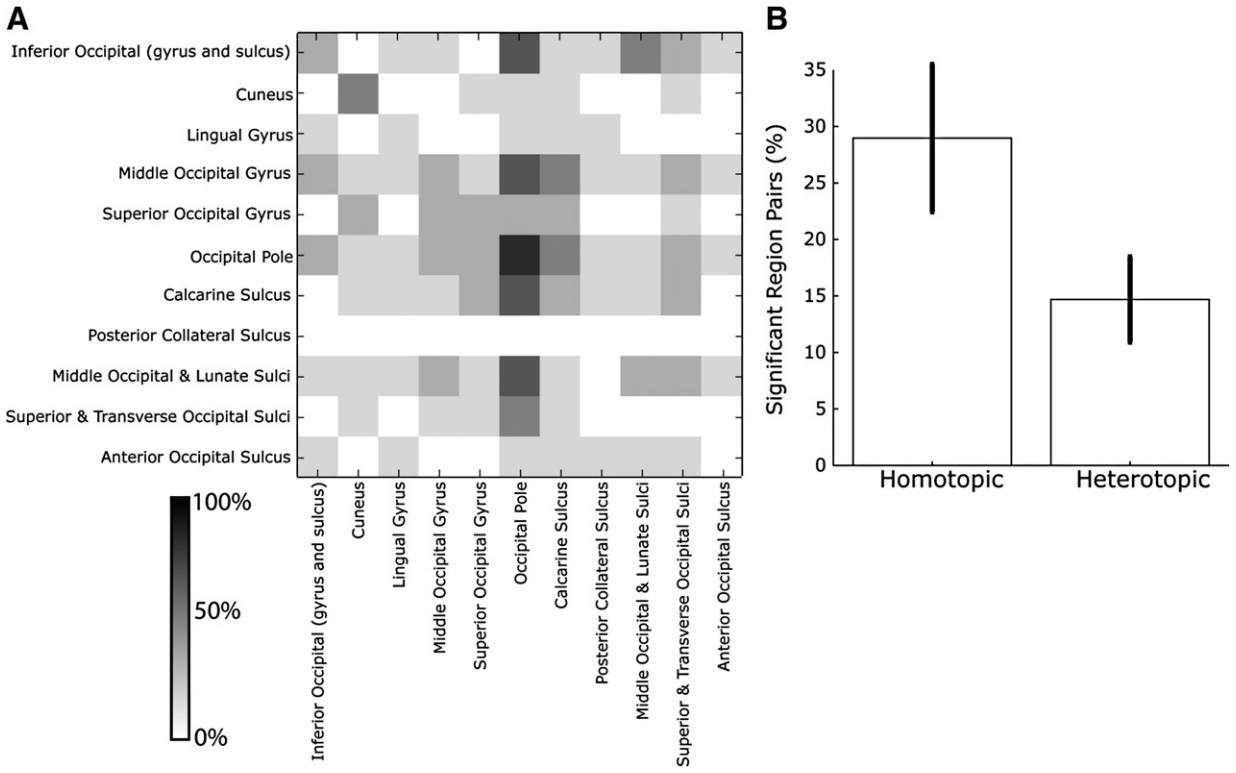

Fig. 5. Occipital lobe connectivity. A) Connectivity matrix, ***C***, for all 11 occipital regions. B) Average number of significant homotopic and heterotopic pairs across subjects. Same plotting conventions as used in Fig. 4.

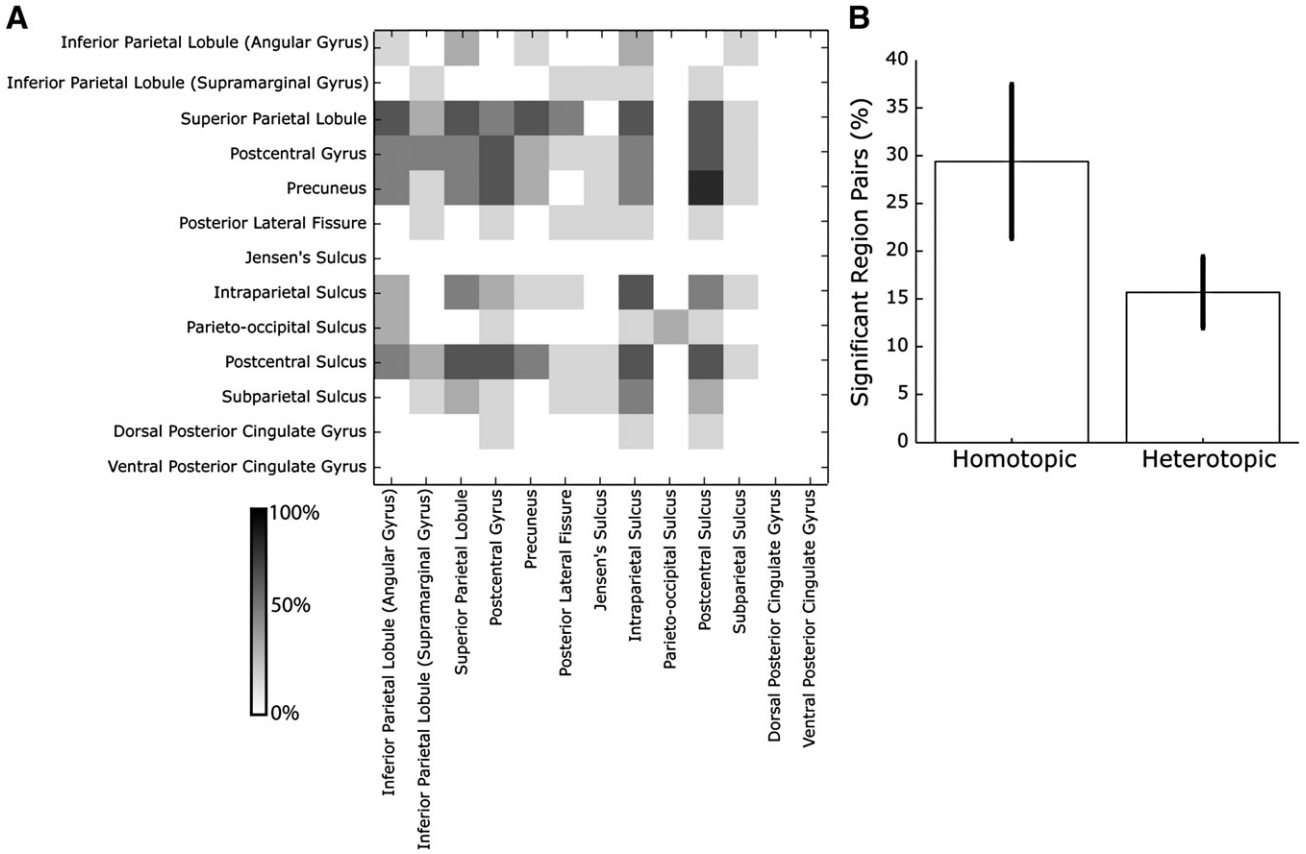

Fig. 6. Parietal lobe connectivity. A) Connectivity matrix, ***C***, for all 13 parietal regions. B) Average number of significant homotopic and heterotopic pairs across subjects. Same plotting conventions as used in Fig. 4.

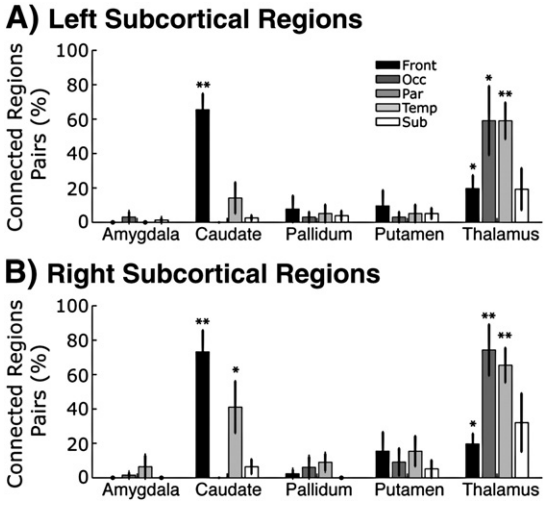

Fig. 7. Connectivity to subcortical nuclei. A) Average number of significant projection pairs from right hemisphere cortical regions to five subcortical ROIs in the left hemisphere. Error bars represent standard error across subjects. B) Same as A, but for left cortical projections to right hemisphere subcortical ROIs. Single asterisks reflect $p<0.025$ and double asterisks reflect $p<0.005$.

the caudate since we found no significant connections to the putamen in any callosal sub-region (all $T(5)<1.75$, p's>0.07). We also found strong, consistent callosal projections to the thalamus. In general, there were strong bilateral connections from the frontal (Left: $T(5)=2.55$, $p<0.025$; Right: $T(5)=3.29$, $p<0.025$), occipital (Left: $T(5)=2.94$ $p<0.025$; Right: $T(5)=4.99$, $p<0.025$) and parietal (Left: $T(5)=5.51$, $p<0.025$; Right: $T(5)=6.48$, $p<0.025$) regions that is consistent with well-established neuroanatomical findings (Nolte, 2002). As expected, we found no significant connections patters to either the amygdala or the pallidum (all $T(5)<1.81$, p's>0.06).

Discussion

We have shown how using a combination of high resolution white matter mapping (i.e., HDFT) with multi-stage tractography can produce a more complete *in vivo* mapping of the corpus callosum than has been previously reported. This allowed us to apply within-subject, permutation statistical methods to quantify patterns of homotopic and heterotopic commissural connectivity between both cortical and subcortical regions in the human brain. The connectivity patterns we observed are in agreement with patterns seen at the level of histological studies of nonhuman primate and post-mortem human brains (Chao et al., 2009; Park et al., 2008; Schmahmann and Pandya, 2006). Using this information we provided the first *in vivo* statistical maps of the sparse and dense connectivity both between and within lobular regions of cortex and subcortical regions.

In order to optimize full coverage of the corpus callosum, we implemented GQI reconstruction on DSI data to provide a more complete resolution of complex fiber crossings that typically hinder diffusion tractography. We were able to visualize the orientation distribution functions of complex triple crossings that caused loss of coverage to posterior callosal pathways (see Fig. 1a). Using a "brute-force", *a priori* ROI tracking approach, similar to what has been described elsewhere (Chao et al., 2009; Huang et al., 2004), we successfully identified specific projections from the posterior neocortex that are often missed with typical tractography approaches. This novel combination of reconstruction and fiber tracking produced results consistent with both current imaging and histological literature, providing new evidence for the validity of such approaches.

It should be pointed out that all diffusion imaging approaches suffer a false-negative detection problem that can affect the interpretation of results, particularly when tracking to certain regions (e.g., the inferior parietal lobule). Indeed, analysis of callosal projections using relatively low-directional DTI methods show considerably less coverage of these pathways than reported in the present study (see Fitsiori et al., 2011). Even with the HDFT approach we employed, there are likely other fiber projections that we are unable to detect in the callosal pathway using diffusion spectrum imaging. Without more histological evidence to unequivocally confirm the topography pattern in humans, the progression of diffusion imaging may remain somewhat constrained. However, even histological measures, restricted mainly to excised post-mortem brains, have their limitations. For example, microsurgical, histological studies of white matter anatomy are confounded by complexity of fiber systems. In some cases, one fiber system must be destroyed in order to reveal another adjacent or underlying system (Fernandez-Miranda et al., 2008). Therefore, integrating *in vivo* imaging methods with microsurgical histological approaches can allow for overcoming the independent limitations of each method. By yielding a consistent pattern of significant interhemispheric connections across subjects, along with an increased spatial resolution, we can further increase the reliability of fiber pathways' detection in imaging and optimize the potential for this multi-modal *in vivo* and *ex vitro* anatomical approach (see following discussion).

Several of the consistent connection patterns that we observed are in agreement with previous literature across anatomical and functional imaging modalities. Due in part to having a larger cortical surface area than parietal and occipital cortices, the frontal lobe showed the greatest amount of overall commissural connectivity. Consistent heterotopic connections of the middle frontal gyrus, where Brodmann's areas 10 and 46 are located, provides structural evidence for the functional role of the dorsal lateral prefrontal cortex as a major center of executive function and the cognitive control network (Miller and Cohen, 2001). Moreover, the high degree of connectivity, especially of the middle frontal gyrus and precentral gyrus, is consistent with the frontal lobe being a densely connected association cortex region (Nolte, 2002).

In addition to the rich interhemispheric connectivity of the frontal lobe that we observed, the posterior parietal cortices, also association cortices, showed a high degree of contralateral connections. Most notably, the distributed pathways between the precuneus and contralateral regions was remarkably consistent with structural (Hagmann et al., 2008) and functional (Cole et al., 2010) connectivity observations, which validates its role as a cortical network hub region (Hagmann et al., 2008). Finally, we were also able to observe significant connectivity between cortical and specific subcortical regions. In particular the caudate (see Chapter 14, Nieuwenhuys et al., 2007) and thalamus (Behrens et al., 2003) connections to contralateral cortical regions are supported by literature. The fact that we observed these pathways and not output pathways of the basal ganglia (i.e., the pallidum) or nuclei known to not project via the corpus callosum (i.e., the amygdala; see Chapter 13, Nieuwenhuys et al., 2007), give us an indication that our results are not merely noise, but do reflect some intrinsic connections.

While our analysis detected several statistically significant connection pathways across subjects, there may still be a substantial likelihood for missing a number of true underlying callosal connections (i.e., Type-II error). By adopting a permutation "bootstrap" approach (Manly, 1997) to determine significant connections within each subject (see Methods subsection Data analysis), we attempted to control for the degree of within-subject noise in the final analysis. However, there was still some degree of individual variation in connections patterns across our sample (see Supplementary Fig. 2). This variability could arise from multiple sources, including noise in the acquisition and analysis stages (Jones and Cercignani, 2010), variations in within subject neuroanatomy, or the stochastic nature of the fiber tractography process itself. Rather than being a limitation, however, this between-subject variability gets directly at the core goal of the current study by explicitly illustrating the degree of variability in detecting specific callosal connections with diffusion imaging methods.

In vivo mapping of the human corpus callosum at this level has the potential to impact both empirical research and clinical applications. Our connectivity maps are the first detailed description of the full connectivity structure in the human corpus callosum and the reliability of detecting these patterns across subjects. These structural patterns can facilitate *a priori* predictions about the functional dynamics of specific interhemispheric networks. In addition, knowing the structural pattern of this pathway in neurologically healthy adults can provide a baseline for understanding changes in patients suffering from white matter pathologies that can affect the corpus callosum, such as Alzheimer's disease (Rose et al., 2000), schizophrenia (Foong et al., 1999) and multiple sclerosis (Coombs et al., 2004). Based on the work by Fernandez-Miranda and colleagues (2008) , given the complimentary advantages of both microsurgical dissection and diffusion imaging based tractography, combining these modalities reflects the best way of validating the progression of novel connection pattern identification in clinical populations. Indeed, by adopting similar permutation statistical analyses as we employ here, we can begin to characterize the confidence of individual connection pairs at the single subject level. This has great potential in the current development of clinical-level diagnostic tools. As white matter imaging tools and histological techniques continue to advance, the resolution and reliability of such mapping can only improve.

Acknowledgments

The authors thank Drs. Juan Fernandez-Miranda and Johnathan Engh for helpful comments provided during this project. This work was supported by DARPA contract NBCHC070104.

Appendix A. Supplementary data

Supplementary data to this article can be found online at doi:10.1016/j.neuroimage.2011.09.056.

References

Behrens, T.E.J., Johansen-Berg, H., Woolrich, M.W., Smith, S.M., Wheeler-Kingshott, C.A.M., Boulby, P.A., Barker, G.J., Sillery, E.L., Sheehan, K., Ciccarelli, O., Thompson, A.J., Brady, J. M., Matthews, P.M., 2003. Non-invasive mapping of connections between human thalamus and cortex using diffusion imaging. Nat. Neurosci. 6, 750–759.

Bloom, J.S., Hynd, G.W., 2005. The role of the corpus callosum in interhemispheric transfer of information: excitation or inhibition? Neuropsychol. Rev. 15, 59–71.

Chao, Y., Cho, K., Yeh, C., Chou, K., Chen, J., Lin, C., 2009. Probabilistic topography of human corpus callosum using cytoarchitectural parcellation and high angular resolution diffusion imaging tractography. Hum. Brain Mapp. 30, 3172–3187.

Clarke, S., Miklossy, J., 1990. Occipital cortex in man: organization of callosal connections, related myelo- and cytoarchitecture, and putative boundaries of functional visual areas. J. Comput. Neurol. 298, 188–214.

Cole, M.W., Pathak, S., Schneider, W., 2010. Identifying the brain's most globally connected regions. NeuroImage 49 (4), 3132–3148.

Coombs, B.D., Best, A., Brown, M.S., Miller, D.E., Corboy, J., Baier, M., Simon, J.H., 2004. Multiple sclerosis pathology in the normal and abnormal appearing white matter of the corpus callosum by diffusion tensor imaging. Mult. Scler. 10, 392–397.

Cummings, J.L., 1993. Frontal-subcortical circuits and human behavior. Arch. Neurol. 50, 873–880.

de Lacoste, M.C., Kirkpatrick, J.B., Ross, E.D., 1985. Topography of the human corpus callosum. J. Neuropathol. Exp. Neurol. 44, 578–591.

Descoteaux, M., Deriche, R., Knosche, T.R., Anwander, A., 2009. Deterministic and probabilistic tractography based on complex fibre orientation distributions. IEEE Trans. Med. Imaging 28, 269–286.

Di Virgilio, G., Clarke, S., 1997. Direct interhemispheric visual input to human speech areas. Human Brain Mapping 5, 347–354.

Di Virgilio, G., Clarke, S., Pizzolato, G., Schaffner, T., 1999. Cortical regions contributing to the anterior commissure in man. Exp. Brain Res. 124, 1–7.

Dougherty, R.F., Ben-Shachar, M., Bammer, R., Brewer, A.A., Wandell, B.A., 2005. Functional organization of human occipital-callosal fiber tracts. Proceedings of the National Academy of Sciences of the United States of America, 102, pp. 7350–7355.

Fallon, J.H., Ziegler, B.T.S., 1979. The crossed corticocaudate projections in the rhesus monkey. Neurosci. Lett. 15, 29–32.

Fernandez-Miranda, J.C., Rhoton Jr., A.L., Alvarez-Linera, J., Kakizawa, Y., Choi, C., de Oliveira, E.P., 2008. Three-dimensional microsurgical and tractographic anatomy of the white matter of the human brain. Neurosurgery 62, 989–1027 SHC.

Fischl, B., Salat, D.H., Busa, E., Albert, M., Dieterich, M., Haselgrove, C., van der Kouwe, A., Killiany, R., Kennedy, D., Klaveness, S., Montillo, A., Makris, N., Rosen, B., Dale, A.M., 2002. Whole brain segmentation: automated labeling of neuroanatomical structures in the human brain. Neuron 33, 341–355.

Fitsiori, A., Nguyen, D., Karentzos, A., Delavelle, J., Vargas, M.I., 2011. The corpus callosum: white matter or terra incognita. Br. J. Radiol. 84, 5–18.

Foong, J., Maier, M., Clark, C.A., Barker, G.J., Miller, D.H., Ron, M.A., 1999. Neuropathological abnormalities of the corpus callosum in schizophrenia: a diffusion tensor imaging study. J. Neurol. Neurosurg. Psychiatry 68, 242–244.

Hagmann, P., Thiran, J.P., Jonasson, L., Vandergheynst, P., Clarke, S., Maeder, P., Meuli, R., 2003. DTI mapping of human brain connectivity: statistical fibre tracking and virtual dissection. NeuroImage 19, 545–554.

Hagmann, P., Cammoun, L., Gigandet, X., Meuli, R., Honey, C.J., Wedeen, V.J., Sporns, O., 2008. Mapping the structural core of human cerebral cortex. PLoS Biol. 6 (7), e159.

Hofer, S., Frahm, J., 2006. Topography of the human corpus callosum revisited—comprehensive fiber tractography using diffusion tensor magnetic resonance imaging. NeuroImage 32, 989–994.

Hofer, S., Merboldt, K., Tammer, R., Frahm, J., 2008. Rhesus monkey and human share a similar topography of the corpus callosum as revealed by diffusion tensor MRI in vivo. Cereb. Cortex 18, 1079–1084.

Huang, H., Zhang, J., van Zijl, P.C.M., Mori, S., 2004. Analysis of noise effects of DTI-based tractography using the brute-force and multi-ROI approach. Magn. Reson. Med. 52, 559–565.

Jones, D.K., Cercignani, M., 2010. Twenty-five pitfalls in the analysis of diffusion MRI data. NMR Biomed. 23, 803–820.

Jones, E.G., Powell, T.P.S., 1969. Connections of the somatic sensory cortex of the rhesus monkey. II: Contralateral connections. Brain 92, 717–730.

Locke, S., Kruper, D.C., Yakoleve, P.I., 1964. Limbic nuclei of thalamus and connections of limbic cortex. 7. Transcallosal connections of cerebral hemisphere with striatum in monkey and man. Arch. Neurol. 11, 571–582.

Manly, B., 1997. Randomization, Bootstrap and Monte Carlo Methods in Biology, 2nd Ed. Chapman and Hall, New York, NY.

Miller, E.K., Cohen, J.D., 2001. An integrative theory of prefrontal cortex function. Annu. Rev. Neurosci. 24, 167–202.

Nieuwenhuys, R., Voogd, J., van Huijzen, C., 2007. Diencephalon: dorsal thalamus, telencephalon: amygdala and claustrum and telencephalon: basal ganglia, In: Nabbe, M.M. (Ed.), The Human Central Nervous System, 4th ed. Springer-Verlag, Berlin Heidelberg, pp. 253–280. 401–426, 427–490.

Nolte, J., 2002. The thalamus and internal capsule: getting to and from the cerebral cortex, In: Shreiner, J. (Ed.), The Human Brain: an Introduction to Its Functional Anatomy, 5th ed. MO: Mosby, St. Louis, pp. 386–409.

Park, H., Kim, J.J., Lee, S., Seok, J., Chun, J., Kim, D.I., Lee, J.D., 2008. Corpus callosal connection mapping using cortical gray matter parcellation and DT-MRI. Human Brain Mapping 29, 503–516.

Rose, S.E., Chen, F., Chalk, J.B., Zelaya, F.O., Strugnell, W.E., Benson, M., Semple, J., Doddrell, D.M., 2000. Loss of connectivity in Alzheimer's disease: an evaluation of white matter tract integrity with colour coded MR diffusion tensor imaging. J. Neurol. Neurosurg. Psychiatry 69, 528–530.

Schmahmann, J.D., Pandya, D.N., 2006. Corpus callosum. In: Stevens, F. (Ed.), Fiber Pathways of the Brain. Oxford University Press, Inc, New York, NY, pp. 485–496.

Selemon, L.D., Goldman-Rakic, P.S., 1988. Common cortical and subcortical targets of the dorsolateral prefrontal and posterior parietal cortices in the rhesus monkey: evidence for a distributed neural network subserving spatially guided behavior. J. Neurosci. 8, 4049–4068.

Tomasch, J., 1954. Size, distribution, and number of fibres in the human corpus callosum. Anat. Rec. 119, 119–135.

Tuch, D.S., 2004. Q-ball imaging. Magn. Reson. Med. 52, 1358–1372.

Verstynen, T., Jarbo, K., Pathak, S., Schneider, W., 2011. In vivo mapping of microstructural somatotopies in the human corticospinal pathways. J. Neurophysiol. 105, 336–346.

Wang, R., Benner, T., Sorensen, A.G., Wedeen, V.J., 2007. Diffusion toolkit: a software package for diffusion imaging data processing and tractography. Paper presented at the Proceedings from the International Society for Magnetic Resonance in Medicine.

Weeden, V.J., Wang, R.P., Schmahmann, J.D., Benner, T., Tseng, W.Y., Dai, G., Pandya, D.N., Hagmann, P., D'Arceuil, H., de Crespigny, A.J., 2008. Diffusion spectrum magnetic resonance imaging (DSI) tractography of crossing fibers. NeuroImage 41, 1267–1277.

Witelson, S.F., 1989. Hand and sex differences in the isthmus and genu of the human corpus callosum. Brain 112, 799–835.

Yeh, F., Wedeen, V.J., Tseng, W.I., 2010. Generalized Q-sampling imaging. IEEE Trans. Med. Imaging 29, 1626–1635.